Ultrasonic investigation on water-saturated porous scatterers under different boundary conditions

Serge Derible, Hervé Franklin

ACOUSTICS 2012

Ultrasonic investigation on water-saturated porous scatterers under different boundary conditions

S. Derible and H. Franklin

LOMC, CNRS UMR 6294, Université Le Havre, 25, rue Philippe Lebon, 76600 Le Havre, France
serge.derible@univ-lehavre.fr

The goal of this paper is to inverse the Biot parameters of some manufactured water-saturated porous material (plate or cylinder). Mainly three cases of boundary conditions are investigated. First, a porous plate with open and sealed pore condition: the normal reflection and transmission coefficients of a given open pore plate are measured. They are compared with the coefficients obtained when the pores of the faces of the plate are sealed with thin quick setting cement. Second, the backscattering coefficient of a porous cylinder is measured. The calibration signal is the signal backscattered by the same cylinder wrapped in a thin Teflon® film. In that case, the cylinder behaves like a "soft" cylinder. Third, a porous plate with different boundary conditions on its faces: the normal reflected signal onto an open pore plate is recorded when the plate is completely immersed in water and when its upper face is in the air. These two experiments allow us to separate the fast and slow echoes on the signal. The last part presents a theoretical study of the Regge trajectories of the resonance families of a porous cylinder when its superficial pores are open or sealed.

1 Introduction

In the frame of Biot's theory [1, 2], this paper deals with the ultrasonic behavior of some water-saturated porous scatterers under different pore sealing conditions of the superficial pores of their interfaces [3]. It points out the influence of the three kinds of waves (fast, slow, transverse) which can propagate in such mediums and estimates the values of some Biot parameters obtained via an inversion procedure. The required recording technique is first described and the experimental results are then discussed for the studied plates and cylinder.

2 Experimental technique

The studied porous target is immersed in a 2000 liter water tank. Whatever the shape of the porous target, cylinder or plate under different boundary conditions, the same experimental setup is used to insonify it normally and record its response.

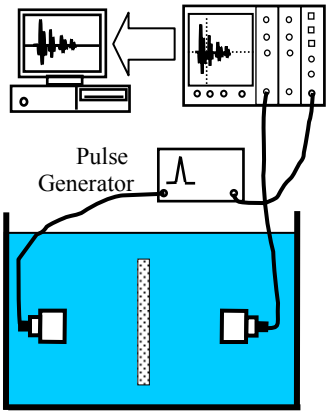

Figure 1: Experimental setup.

The distance between the broadband transducers is about 1 m and the distance between the emitter and the target is about 50 cm. Each of the scatterers is insonified with a normal incident pulse repeatedly launched by the emitter and produced by the 300 V discharge of the internal capacitor of the generator which also triggers the launching. The frequency domain investigated depends of the central frequency of the pair of transducers used (Panametrics®, non-focused, 500 kHz, 1MHz). The signals (reflected and transmitted signals from a plate, backscattered signals by a cylinder) are stored after the electronic perturbations have been strongly reduced thanks to an average of 200 acquisitions. The sampling frequency is 100 MHz and the recorded signals have 80,000 samples.

3 Porous plate

The inversion of the Biot parameters of a porous plate is based on the comparison of the theoretical reflection and transmission coefficients and the experimental complex ones. Each of those latter is obtained via a relevant calibration signal. It is the direct signal from the emitter to the receiver (the plate is simply removed) for the transmission, and the reflected signal onto the water/air interface insonified normally thanks to a mechanical device, not presented in fig. 1, which enables the emitter to be rotated.

The experimental transmission coefficient is the ratio of the Fourier transform of the transmitted signal to the Fourier transform of the incident signal onto the plate. This latter is obtained by shifting the recorded direct signal of the delay time $-d/c_1$ (d is the thickness of the target and c_1 is the velocity of sound in water). The experimental reflection coefficient is the ratio of the Fourier transform of the reflected signal onto the plate to the Fourier transform of the reflected signal onto water/air interface (the obtained complex value is then multiplied by –1 which is the value of the reflection coefficient of the water/air interface). Diffraction can be neglected because those ratios of Fourier transforms are issued from temporal signals recorded under identical geometrical configurations regarding the transducers and the targets. The experimental coefficients are compared to the theoretical ones obtained from a plane wave model.

3.1 Temporal signals

We use commercially available porous plates ($350\,\text{mm} \times 200\,\text{mm} \times 5\,\text{mm}$) made with a thermal-hardened silica grains material named QF20 and produced by Ferros®.

Two identical water-saturated porous plates are successively investigated: one with open pores and the second with its superficial pores of both sides sealed by a thin coat of quick setting cement. In figure 2 the direct signal and the transmitted ones through those plates are plotted.

One can recognize two parts on these signals: a first part similar in shape with the direct signal and then some emerging echoes due to internal reflections of the fast and slow waves onto the faces of the plates. On the whole, the signal issued from the sealed pore plate is simpler because the internal slow wave is strongly reduced by sealing the superficial pores of the plate.

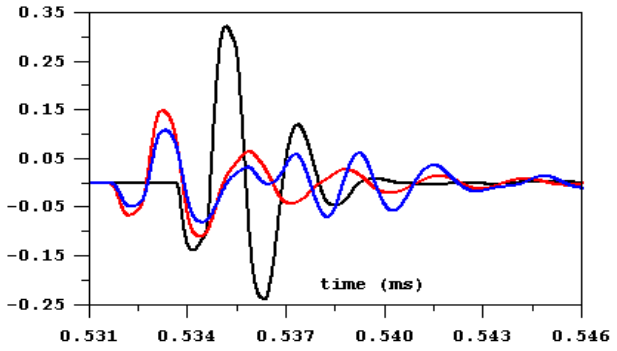

Figure 2: Direct signal (black). Transmitted signals by the plate with open pores (blue) and by the plate with sealed superficial pores (red).

3.2 Reflection, transmission coefficients

In the figures below the reflection and transmission coefficients of the previous plates are compared in a wide frequency range obtained thanks to the association of the spectra given by pairs of identical transducers (central frequency 500 kHz, and 1 MHz) used following the previous experimental procedure presented above.

As usual, the resonances are located where troughs appear on a reflection coefficient while they are located by peaks on a transmission coefficient. The frequency intervals between a selected kind of resonances lead to the value of the celerity of the related wave. So the plots below show that within the sealed pore plate almost only the fast wave propagates while the two longitudinal waves propagate in the open pore plate. In both the studied cases, the influence of the slow wave progressively vanishes as frequency increases.

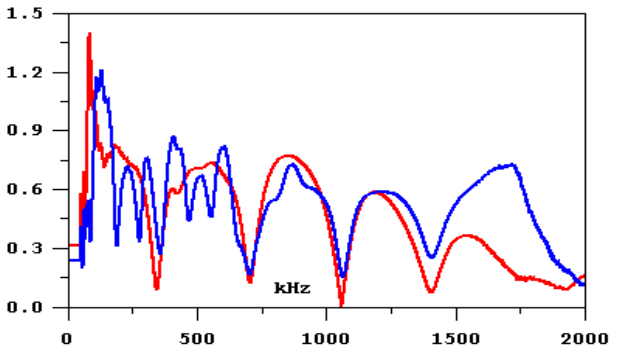

Figure 3: Modulus of the normal reflection coefficient of the open pore plate (blue) and sealed pore plate (red).

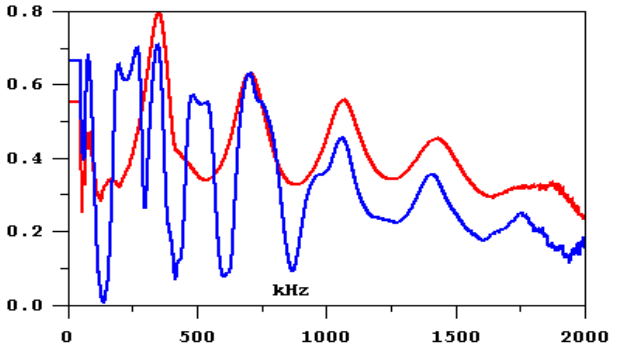

Figure 4: Modulus of the normal transmission coefficient of the open pore plate (blue) and sealed pore plate (red).

Biot's theory is used to inverse the parameters of the porous material of the plate. Figure 5 shows a good agreement between theoretical and experimental transmission coefficients of the QF20 plate. The values found for the parameters are gathered in table I below.

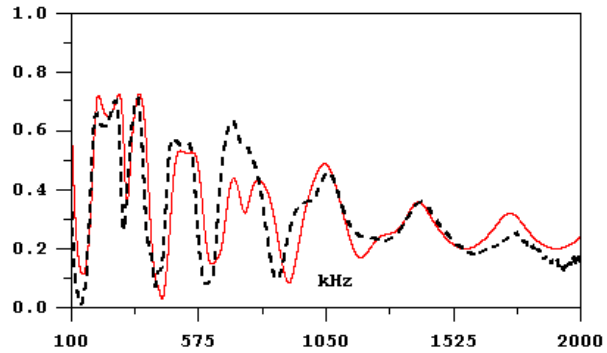

Figure 5: Transmission coefficient of the 5mm QF20 plate (open pores): experimental (dotted line); calculated (red).

4 Porous cylinders

We use commercially available cylinders (15.2 mm in length and 8 mm in diameter) made with a thermal-hardened alumina grains material named FAO30 and produced by Ferros® too. We investigate the normalized backscattered pressure of porous cylinders insonified by an incident plane wave perpendicular to their axis. Here, using the reflected signal onto the water/air interface as a calibration signal is not possible. Because unlike any large plane target, only one part of the pulse launched by the emitter (4 cm in diameter) is incident onto the cylinder and with incidence angles running from 0 to $\pi/2$. That is the reason why the calibration of the backscattered signal of a porous cylinder is achieved thanks to the signal backscattered by the same porous cylinder wrapped in a thin Teflon® film, insonified with the same incident pulse and recorded with the same electronic apparatus chain. In the following, we call experimental diffusion coefficient the ratio of the Fourier transform of the backscattered pressure by the cylinder to the Fourier transform of the backscattered pressure of the wrapped cylinder. The determination of the Biot parameters of the FAO30 material is achieved by finding the best fit between experimental and calculated diffusion coefficients. (See table I, below).

4.1 Temporal signals and results

Let us consider a cylinder of radius a immersed in a fluid in which sound travels with the velocity c_0. Its backscattered pressure is obtained in two times: first, expanding the incident pressure in the usual modal series:

$$p_{inc}(r,\pi) = P_0 e^{-i\omega t} \sum_{n=0}^{\infty} \varepsilon_n i^n J_n(k_0 r)\cos(n\pi), \qquad (1)$$

and second, adding the backscattered pressures of the different modes via the strain stress relations obeyed at the water/porous interface. This leads to the general formula

$$p_{diff}(r,\pi) = P_0 e^{-i\omega t} \sum_{n=0}^{\infty} \varepsilon_n i^n d_n H_n^{(1)}(k_0 r)\cos(n\pi), \qquad (2)$$

where $k_0 = \omega/c_0$ and d_n only depends of the scatterer. For the soft cylinder it equals this ratio of the Bessel and Hankel functions:

$$d_n = -\frac{J_n(k_0 a)}{H_n^{(1)}(k_0 a)}, \quad (3)$$

while it is the solution of a (4×4) matrix equation satisfied by the scalar and vector potentials for a porous cylinder.

The following figures 6, 7 show the evidence of the behavior of a Teflon® coated cylinder as a "soft" cylinder, that is, a cylinder the incident wave onto cannot penetrate as in the case of the water/air interface. Teflon is water-repellent and isolates the porous material from the incident pressure which vanishes on its surface.

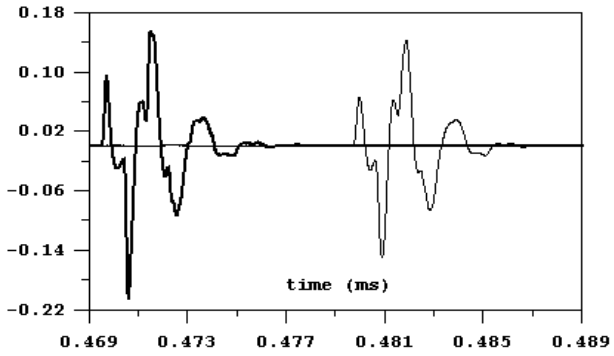

Figure 6: Temporal signals recorded thanks to a 500 kHz central frequency transducer: reflection onto the water/air interface (bold line) and backscattered by a cylinder whose pores are sealed by a Teflon® tape (thin line). The amplitude of this latter is multiplied by 10, for convenience.

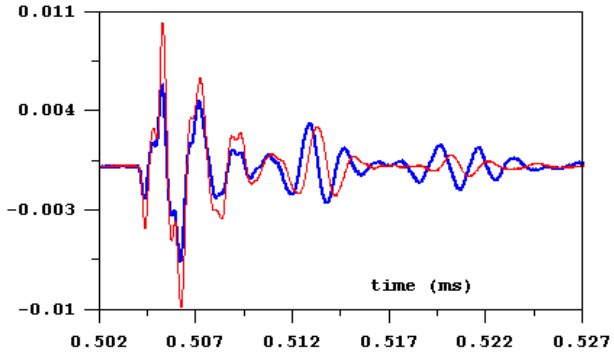

Figure 7: Temporal signal backscattered by an open pore cylinder (blue), sealed pore cylinder (red).

The inversion leads to a frequency-dependence for the permeability of the two studied material.

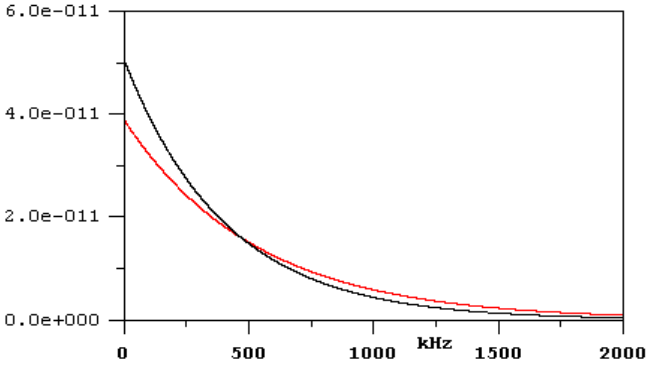

Figure 8: Permeability: QF20 (red), FAO30 (black)

The bulk and shear modulus of the dry porous material have constant complex values.

Table I: Parameters of the constituting porous material of the studied targets.

Parameter	QF20	FAO30	Unity
Tortuosity	2	2.35	
Porosity	0.4	0.3	
Water viscosity	1.110^{-3}	1.110^{-3}	kg $m^{-1}s^{-1}$
Permeability	See Fig. 8		m^2
Mean radius of the pores	35	45	µm
Bulk modulus of the grains	$(36.6+0i)$	$(228+0i)$	GPa
Bulk modulus of the dry material	$(12+0.6i)$	$(32+0.85i)$	GPa
Shear modulus of the dry material	$(6.6+0.37i)$	$(15+0.8i)$	GPa

5 Slow wave

In order to check if an unknown porous material obeys Biot's theory, it is often set up a simple experiment in which fast and slow echoes are well separated and so, the evidence of a slow wave is exhibited. The previous experimental setup is used to insonify normally the water/air interface. The immersed porous plate (1cm thick) is placed with its second face in contact with air. The normal incident wave produces slow and fast waves inside the plate. The strain stress relations for the second interface show that there is no wave conversion if the transmission coefficient is zero. This configuration enhances the reflected waves and makes the localization of the different echoes easier.

The recorded signal is presented in Fig. 9. One can easily recognize the specular echo onto the water/porous interface followed by three decreasing fast echoes and then the first slow echo whose amplitude is stronger than that of the third fast echo.

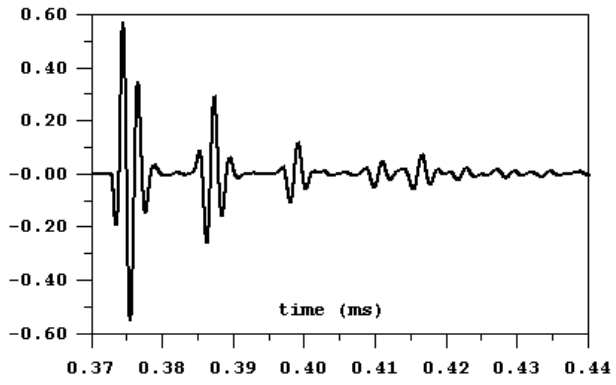

Figure 9: Reflected signal onto the porous plate with its upper face in contact with air. The central frequency of the transducer is 500 kHz.

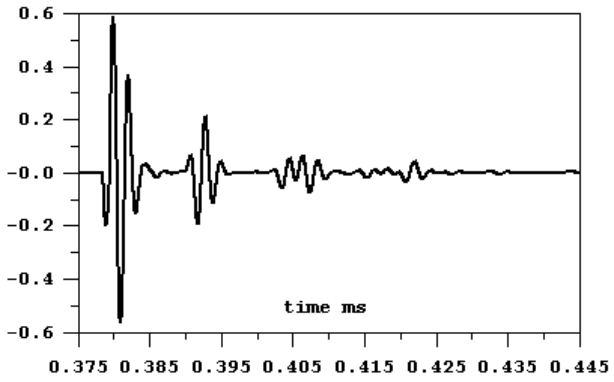

Figure 10: Reflected signal onto the immersed porous plate. The central frequency of the transducer is 500 kHz.

Figure 10 shows the reflected signal onto the previous porous plate when it is completely immersed. The recognition of the different waves is not so easily carried out than in Fig. 9. Except for the specular echo, the amplitudes are smaller because now a part of the incident energy is transmitted in water and wave conversion of the fast and slow echoes onto the inner interfaces of the plate takes place. Another consequence is the overlapping of those more numerous echoes.

6 Dispersion equations of porous QF20 cylinders

6.1 Open pore boundary conditions

The complex eigenfrequencies of the porous cylinder correspond to the roots $x_0 = k_0 a$ of the dispersion equation $D_n^o(x_0) = 0$ (see Appendix). The physical parameters of water and of the QF-20 material used in the computations are given in Ref. 3. The radius of the cylinder is $a = 0.395 \times 10^{-2}$ m. For each mode n, there appear two multiplicities $l = 1, 2, ...$ and $m = 1, 2...$ of eigenfrequencies that account for the various radial deformations of the contour of the scatterer. It can be noticed that no $(0, m)$ modes have been found.

The Regge trajectories [4] (real parts of eigenfrequencies versus mode number) of the family l can be found approximately by solving the dispersion equation (4)

$$\rho_{f2} x_0 H_n^{(1)\prime}(x_0) J_n(x_2) - \rho_0 x_2 H_n^{(1)}(x_0) J_n'(x_2) = 0 \qquad (4)$$

of an immersed lossy fluid cylinder of density ρ_{f2} and wavenumber ℓ_2 (theses two parameters are those of the slow wave). The Regge trajectories are presented in Fig. 11. Computations not presented here showed that curves labeled m in Fig. 11 have trajectories very close to those obtained by solving the dispersion equation of an immersed dissipative elastic cylinder (density ρ_t, wavenumbers ℓ_2 and ℓ_t). It can be noted that these approximations work for the real parts of the eigenfrequencies, not necessarily for the imaginary parts.

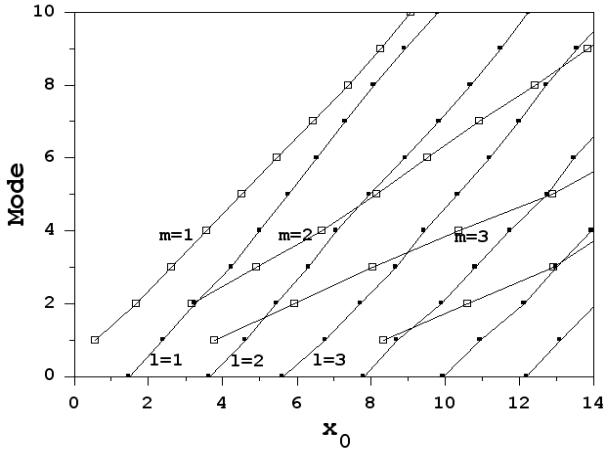

Figure 11. Regge trajectories of the first families of resonances for a QF-20 porous cylinder with open pores. Empty boxes : *m* family. Filled boxes : *l* family

6.2 Sealed pore boundary conditions

The complex eigenfrequencies correspond to the roots x_0 of the dispersion equation $D_n^s(x_0) = 0$. As for the open pore case, the Regge trajectories presented in Fig. 12 exhibit two families of curves, l and m.

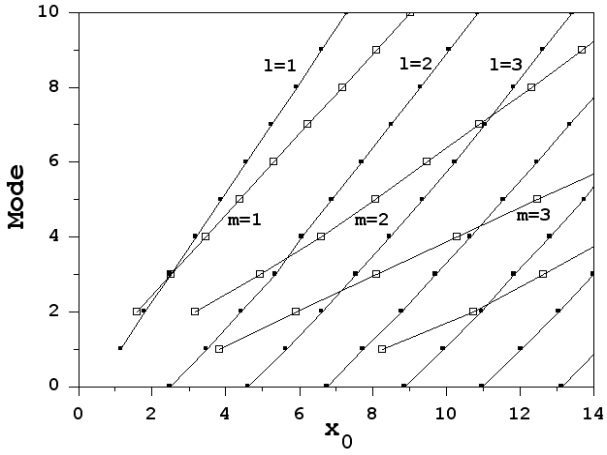

Figure 12. Regge trajectories of the first families of resonances for a QF20 porous cylinder with sealed pores. Empty boxes: *m* family. Filled boxes: *l* family.

Here, because of the sealing of the superficial pores, the radial fluid to solid displacement is null at r = a. Therefore, the identification of the porous cylinder response to that of a lossy fluid column (density ρ_{f2}, wavenumber ℓ_2 of slow waves) yields the following dispersion equation

$$J_n'(x_2) = 0. \qquad (5)$$

The real parts of the eigenfrequencies found by solving Eq. (4) are very close to curves labeled l in Fig. 12. Curves labeled m in Fig. 12 look like those in Fig. 11 and it can be concluded that the boundary conditions (open or sealed pores) do not affect significantly the m curves. It's the contrary for the l curves since strong shifts can be observed between Figs. 11 and 12. It is also important to note that the l curves are due to the slow wave exclusively.

The phase velocity $c^p(\alpha, x_0)$ and the critical angle of excitation θ_α^0 of the α^{th} circumferential wave ($\alpha = l$ or $\alpha = m$) can be found according to the formula [5]

$$c^p(\alpha, x_0) = c_0\left(x_0 / \mathrm{Re}\{n_\alpha(x_0)\}\right) = \theta_\alpha^0(x_0), \quad (6)$$

where n_α is the corresponding value of the mode number n, which is now considered as a complex continuous variable. In Fig. 13, the dispersion curves of the relative phase velocity $c^p(\alpha, x_0)/c_0$ are presented for $\alpha = l$ and $\alpha = m$.

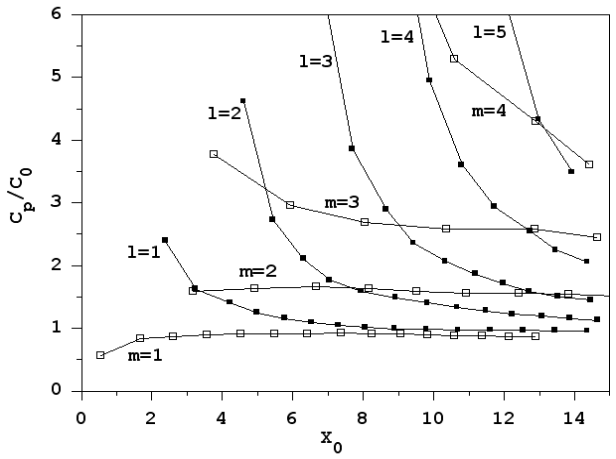

Figure 13. Dispersion curves of relative phase velocities for open pore conditions

7 Conclusion

Both theoretical and experimental results were obtained for fluid-saturated porous targets having hydraulic conditions at the interfaces. It was shown that the study of the resonances of such structures must include also the study of simpler models, fluid and elastic cylinders. Open pore conditions and sealed pore conditions lead in the same frequency range, to a different number of resonances since the l resonances can be strongly shifted when the conditions change. As a consequence, a crossing between the $m = 1$ curve and the $l = 1$ curve occurs. The resonances in the form functions, although numerous, are easily recognizable. Experiments show that resonances can be detected in spite of the strong dissipations in the porous material.

Appendix: **Dispersion equations** $D_n^o(x_0) = 0$**, and** $D_n^s(x_0) = 0$. The dispersion equation $D_n(x_0) = 0$ for a fluid saturated porous cylinder immersed in the same fluid is obtained by application of the boundary conditions at the interface $r = a$. It must account for the admittance parameter κ_s characterizing the interface permeability [3, 6]. Calculations show that

$$D_n = \begin{vmatrix} a_{n,11} & a_{n,12} & a_{n,13} & a_{n,14} \\ a_{n,21} & a_{n,22} & a_{n,23} & a_{n,24} \\ a_{n,31} & a_{n,32} & a_{n,33} & a_{n,34} \\ 0 & a_{n,42} & a_{n,43} & a_{n,44} \end{vmatrix}$$

with

$$a_{n,11} = -\rho_{0t} x_t^2 H_n^{(1)}(x_0),$$
$$a_{n,12} = 2x_1 J_n'(x_1) + \left(\rho_{1t} x_t^2 - 2n^2\right) J_n(x_1),$$
$$a_{n,13} = 2x_2 J_n'(x_2) + \left(\rho_{2t} x_t^2 - 2n^2\right) J_n(x_2),$$
$$a_{n,14} = -2n J_n(x_t) + 2x_t J_n'(x_t),$$
$$a_{n,21} = -x_0 H_n^{(1)\prime}(x_0),$$
$$a_{n,22} = (1+\gamma_1) x_1 J_n'(x_1),$$
$$a_{n,23} = (1+\gamma_2) x_2 J_n'(x_2),$$
$$a_{n,24} = -(1+\gamma_t) n J_n(x_t),$$
$$a_{n,31} = -H_n^{(1)}(x_0),$$
$$a_{n,32} = \frac{\rho_{f1}}{\rho_0} J_n(x_1) + \frac{i}{\rho_0 \kappa_s \omega a} \gamma_1 x_1 J_n'(x_1),$$
$$a_{n,33} = \frac{\rho_{f2}}{\rho_0} J_n(x_2) + \frac{i}{\rho_0 \kappa_s \omega a} \gamma_2 x_2 J_n'(x_2),$$
$$a_{n,34} = -\frac{i}{\rho_0 \kappa_s \omega a} n \gamma_t J_n(x_t),$$
$$a_{n,42} = 2n\left[x_1 J_n'(x_1) - J_n(x_1)\right],$$
$$a_{n,43} = 2n\left[x_2 J_n'(x_2) - J_n(x_2)\right],$$
$$a_{n,44} = \left(x_t^2 - 2n^2\right) J_n(x_t) + 2x_t J_n'(x_t),$$

J_n ($H_n^{(1)}$ resp.) denote Bessel (Hankel resp.) functions, J_n', $H_n^{(1)\prime}$ the derivatives with respect to their arguments, ω denotes the angular frequency, $\rho_{jt} = \rho_j/\rho_t$, $x_j = \ell_j a$ ($j = 0, 1, 2$), $\rho_{0t} = \rho_0/\rho_t$. The other quantities are defined in Ref. 6. If $\kappa_s \to \infty$ (open pores), $D_n(x_0) \to D_n^0(x_0)$. If $\kappa_s \to 0$ (sealed pores), $D_n(x_0) \to D_n^s(x_0)$.

8 Reference

[1] M. A. Biot, "Theory of propagation of elastic waves in a fluid saturated porous solid. I. Low frequency range," J. Acoust. Soc. Am. 28, 168-178 (1956).

[2] .M. A. Biot, "Theory of propagation of elastic waves in a fluid saturated porous solid. II. High frequency range," J. Acoust. Soc. Am. 28, 168-178 (1956).

[3] H. Franklin, S. Derible, C. Popa, "Expansions of reflected-transmitted signals to estimate the slow wave strength in fluid-saturated porous layers", J. Acoust. Soc. Am. 128 (3) 1073-1086 (2010).

[4] L. Flax, L. R. Dragonette, H. Überall, "Theory of elastic resonance excitation by sound scattering", J. Acoust. Soc. Am. **63** 723-731 (1978).

[5] J.-L. Rousselot, " Champ diffusé par un cylindre fluide: Comparaison entre la théorie géométrique de la diffraction et la théorie modale," ACUSTICA 80, 14-27 (1994).

[6] F. Luppé, J.-M. Conoir, H. Franklin," Scattering by a fluid cylinder in a porous medium: Application to trabecular bone ", J. Acoust. Soc. Am. 111 (6) 2573-2582 (2002).